ACS OMEGA

http://pubs.acs.org/journal/acsodf

Article

Crystal Structure of the [4Fe−4S] Cluster-Containing Adenosine-5′-phosphosulfate Reductase from *Mycobacterium tuberculosis*

Patricia R. Feliciano, Kate S. Carroll, and Catherine L. Drennan*

Cite This: *ACS Omega* 2021, 6, 13756−13765

Read Online

ACCESS | Metrics & More | Article Recommendations | Supporting Information

ABSTRACT: Tuberculosis (TB) is the deadliest infectious disease in the world. In *Mycobacterium tuberculosis*, the first committed step in sulfate assimilation is the reductive cleavage of adenosine-5′-phosphosulfate (APS) to form adenosine-5′-phosphate (AMP) and sulfite by the enzyme APS reductase (APSR). The vital role of APSR in the production of essential reduced-sulfur-containing metabolites and the absence of a homologue enzyme in humans makes APSR a potential target for therapeutic interventions. Here, we present the crystal structure of the [4Fe−4S] cluster-containing APSR from *M. tuberculosis* (MtbAPSR) and compare it to previously determined structures of sulfonucleotide reductases. We further present MtbAPSR structures with substrate APS and product AMP bound in the active site. Our structures at a 3.1 Å resolution show high structural similarity to other sulfonucleotide reductases and reveal that APS and AMP have similar binding modes. These studies provide structural data for structure-based drug design aimed to combat TB.

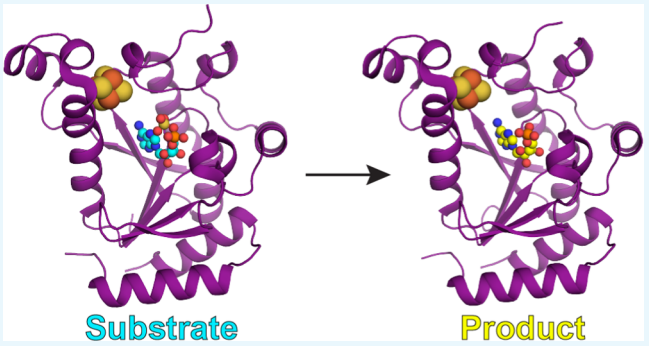

INTRODUCTION

Mycobacterium tuberculosis is a bacterium that causes tuberculosis (TB) disease. Infections with *M. tuberculosis* can evolve from latent TB infection, which is an asymptomatic and non-transmissible state, to a contagious active state of TB disease (pulmonary TB) that can lead to death.[1] The World Health Organization (WHO) estimated that TB causes 1.5 million deaths annually, making TB one of the top 10 causes of death worldwide. The TB epidemic has been aggravated by the prevalence of drug-resistant bacteria. According to the WHO, approximately 200,000 new cases of TB in 2019 were resistant to the first-line drug rifampicin or displayed multidrug resistance. Thus, there is an urgent need to develop new therapies to combat multidrug-resistant TB infection.

The sulfate assimilation pathway provides reduced sulfur for the biosynthesis of cysteine, which is the source for a variety of reduced-sulfur-containing metabolites such as methionine, coenzyme A, mycothiol, and lipoic acid.[2] These essential metabolites play a critical role in the survival, pathogenesis, and antioxidant defense of persistent and drug-resistant *M. tuberculosis*.[3,4] In *M. tuberculosis*, the first committed step in the sulfate assimilation pathway is the conversion of adenosine-5′-phosphosulfate (APS) to adenosine-5′-phosphate (AMP) and sulfite (Scheme 1). This reaction is catalyzed by the enzyme APS reductase (APSR) with reducing equivalents from thioredoxin (Trx). *M. tuberculosis* APSR (MtbAPSR, EC:1.8.4.8, UniProt P9WIK3, NCBI reference sequence WP_003412303.1) is a [4Fe−4S] cluster-containing enzyme that is critical for *M. tuberculosis* survival in the chronic infection phase and affords protection from oxidative stress.[3] Additionally, humans do not have an APSR homologue. Therefore, the enzyme MtbAPSR is an attractive target for the development of anti-TB therapies.

Some organisms, such as *Escherichia coli* and *Saccharomyces cerevisiae*, reduce 3′-phosphoadenosine-5′-phosphosulfate (PAPS) instead of APS to form 3′-phosphoadenosine-5′-phosphate (PAP) instead of AMP and sulfite.[5,6] The enzyme responsible is PAPS reductase (PAPSR), which does not contain an Fe−S cluster as a cofactor. Although the sequence identity between APSR and PAPSR enzymes is modest (25−33%) and displays differences in substrate specificity and cofactor usage, the chemistry catalyzed is largely the same. The proposed catalytic mechanism for APSR and PAPSR enzymes consists of the nucleophilic attack of a catalytic cysteine at the sulfur atom of APS or PAPS to form an enzyme−thiosulfonate intermediate (E-Cys-Sγ-SO_3^-), followed by Trx-mediated sulfite release[7] (Scheme 2). The catalytic cysteine is part of a conserved ^{248}E**C**G(L/I)H^{252} motif (Mtb numbering) that is found on the mobile C-terminal tail of the protein. This C-terminal tail also contains a ^{237}R(S/E/A)GR(W/F)^{241}

Received: February 25, 2021
Accepted: April 28, 2021
Published: May 17, 2021

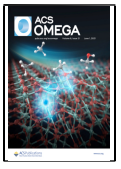

Scheme 1. Reaction Catalyzed by APSR

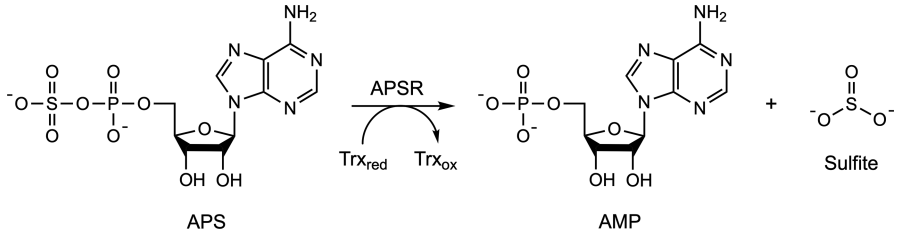

Scheme 2. Sulfonucleotide Reduction Mechanism

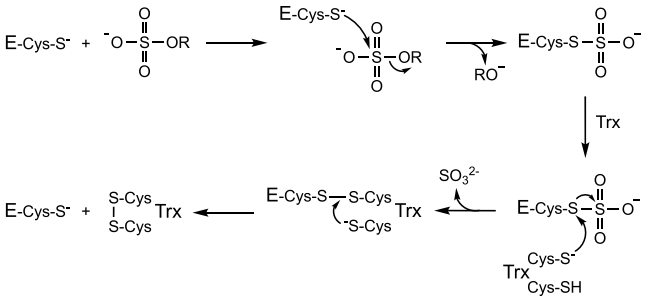

substrate-binding motif and is known to function as a lid to the active site cavity.[8] Structural studies have suggested that the C-terminal tail is displaced to allow for substrate binding, and then the tail arranges to close the active site when the enzyme−thiosulfonate intermediate is formed and then moves again to reopen the active site to release AMP or PAP and to allow for Trx-catalyzed sulfite release.[8−10] Biochemical studies of MtbAPSR showed that the substitution of conserved C249 with serine resulted in enzyme inactivation and no formation of the enzyme−thiosulfonate intermediate, indicating that C249 functions as the C-terminal catalytic residue.[7] The [4Fe−4S] cluster has been shown to be essential for catalysis, although its role remains unknown.[11,12]

Here, we report the crystal structures of holo-([4Fe−4S] cluster-bound) MtbAPSR, with substrate APS and with product AMP. Our structures provide a starting place for structure-based drug design efforts targeting TB infection.

RESULTS AND DISCUSSION

Overall Structure of MtbAPSR. The crystal structure of holo-MtbAPSR was determined at a 3.1 Å resolution by single-wavelength anomalous dispersion (SAD) phasing using the data collected at the iron peak wavelength (Tables 1 and 2). Two additional 3.1 Å resolution structures of MtbAPSR were determined by molecular replacement, one with substrate APS and the other with product AMP (Tables 1 and 2). The asymmetric unit in all cases contains two copies of the monomeric enzyme (chains A and B). However, both interface and quaternary structure analyses using protein interfaces, surfaces, and assemblies (PISA)[13] and previous biochemical data suggest that MtbAPSR is monomeric.[7] All three MtbAPSR structures described here are highly similar to each other, with a root-mean-square deviation (rmsd) between 0.24 and 0.56 Å for all of the Cα atoms (Table S1).

The MtbAPSR monomer contains 6 β-strands (β1 to β6) and 13 α-helices (α1 to α13) that fold into a single domain with a central six-stranded β-sheet surrounded by α-helices (Figures 1A,B and S1). The first ∼4 N-terminal residues, the flexible loop between α2 and β1 (G44 to G55), and the last ∼24 C-terminal residues (A231 to S254), which contain the catalytic C249, were excluded from the structures due to the lack of interpretable electron density. The monomer has a [4Fe−4S] cluster coordinated by four cysteine residues from α7 (C140 and C141) and α13 (C223 and C226) with a C-C-X_{81}-C-X_2-C motif (Figure 1D). The electrostatic surface potential of the MtbAPSR monomer reveals a positively charged deep cavity located below the [4Fe−4S] cluster. It is within this cavity that residues of the active site are located (Figure 1C).

Structural Comparisons between MtbAPSR and Related Structures. A search in the Protein Data Bank (PDB) using the DALI server[15] identified four entries with high structural similarity to MtbAPSR (Z-score > 20; rmsd ∼2 Å for ∼200 Cα atoms) (Table 1): *Pseudomonas aeruginosa* APSR (PaAPSR; PDB code 2GOY[8]), *E. coli* PAPSR (EcPAPSR; PDB code 2O8V[9]), *S. cerevisiae* PAPSR (ScPAPSR; PDB code 2OQ2[10]), and *Physcomitrella patens* APSR-B (PpAPSR-B; PDB code 4BWV[16]), which is an APSR enzyme with no [4Fe−4S] cluster. These four enzymes and MtbAPSR share relatively low amino acid sequence identity (25−33%) (Figure S2) despite their high structural similarity. Superpositions of these four structures with MtbAPSR show that the main structural differences are found in the N-terminal region that includes helix α1, which has a different length and/or position in all five of these enzymes (Figures 2 and S3). These variations in the N-terminal region appear to impact the oligomeric states that these enzymes form. MtbAPSR is monomeric,[7] whereas PaAPSR is homotetrameric[8] (Figure 3A), and EcPAPSR, ScPAPSR, and PpAPSR-B form three

Table 1. Structural Data Available for APSR and PAPSR Enzymes

structures	resolution (Å)	rmsd (Å) between MtbAPSR and related structures	oligomeric state	cofactor	ligand	C-terminal tail
MtbAPSR (this work)	3.1		monomer	[4Fe−4S]	APS AMP	disordered
PaAPSR (PDB 2GOY)	2.7	1.3	tetramer	[4Fe−4S]	APS	partially ordered
ScPAPSR (PDB 2OQ2)	2.1	1.7	dimer	no cluster	PAP	ordered
EcPAPSR (PDB 2O8V)	3.0	1.35	dimer	no cluster	no ligand	partially ordered
PpAPSR-B (PDB 4BWV)	1.8	1.6	dimer	no cluster	no ligand	partially ordered

https://doi.org/10.1021/acsomega.1c01043
ACS Omega 2021, 6, 13756−13765

Table 2. Data Collection and Refinement Statistics of MtbAPSR

data name	MtbAPSR-SAD[a]	MtbAPSR-native	MtbAPSR-APS	MtbAPSR-AMP
soaking			APS	AMP
ligand in the structure			APS	AMP
PDB ID		7LHR	7LHS	7LHU
		Data Collection		
Space group	$P4_32_12$	$P4_32_12$	$P4_32_12$	$P4_32_12$
Cell dimensions				
a, *b*, *c* (Å)	77.74, 77.74, 204.51	77.41, 77.41, 204.35	77.50, 77.50, 205.31	77.70, 77.70, 206.36
α, *β*, *γ* (°)	90, 90, 90	90, 90, 90	90, 90, 90	90, 90, 90
wavelength (Å)	1.7389	0.9792	0.9791	0.9792
resolution (Å)	50−3.45 (3.51−3.45)[b]	50−3.1 (3.15−3.1)[b]	50−3.1 (3.15−3.1)[b]	50−3.1 (3.15−3.1)[b]
no. of unique reflections	8,838	11,937	11,945	12,260
R_{sym}	0.248 (3.276)[b]	0.134 (1.900)[b]	0.143 (1.685)[b]	0.149 (1.710)[b]
$I/\sigma(I)$	22 (1.0)[b]	32.4 (1.0)[b]	23.6 (0.9)[b]	36 (1.0)[b]
CC1/2[d]	(0.514)[b]	(0.616)[b]	1.001 (0.597)[b]	1.002 (0.525)[b]
completeness (%)	100 (100)[b]	100 (99.6)[b]	99.5 (94.2)[b]	99.9 (98.5)[b]
redundancy	29.4 (15.8)[b]	23.3 (13.9)[b]	13.6 (7.5)[b]	19.2 (9.5)[b]
		Refinement		
no. of reflections used		11,826 (1,172)[b]	11,812 (1,091)[b]	12,173 (1,161)[b]
R_{work}/R_{free}[c]		0.2073/0.2492	0.2190/0.2639	0.2297/0.2617
no. of atoms in asu				
protein		3,117	3,133	3,185
no. of molecules				
[4Fe−4S] clusters		2	2	2
APS			2	
AMP				2
MES		2	2	2
water		6	6	7
average B-factors (Å^2)				
protein—chain A		101.3	108.4	104.9
protein—chain B		112.3	121.0	115.9
[4Fe−4S] clusters		85.9	112.5	95.9
MES		94.1	98.1	106.7
APS			113.9	
AMP				106.5
water		69.6	72.8	95.2
r.m.s deviations				
bond lengths (Å)		0.003	0.002	0.002
bond angles (deg)		0.61	0.51	0.52
Ramachandran analysis[e] (%)				
favored		96.6	98.1	98.8
allowed		3.4	1.9	1.2
outliers		0	0	0

[a]Bijvoet pairs were not merged during data processing. [b]Highest resolution shell is shown in parentheses. [c]R_{free} was calculated with 5% of the data. [d]Overall CC1/2 was not available from the version of HKL2000 that was used to process MtbAPSR-SAD and native data sets. [e]Distribution of dihedral angles in the Ramachandran diagram was calculated with the *MolProbity* program.[27]

different homodimeric−oligomeric states[5,16,17] (Figure 3B−D). The unique homodimer formed by PpAPSR-B is due to an unusually long N-terminal helix that superimposes with helix *α*2 (not helix *α*1 of the other structures) and forms the dimer interface (Figures 2D, 3D, and S3D). ScPAPSR uses its helix *α*1 to form a homodimer (Figure 3C) that Ec, Mtb, and Pa APSRs cannot form due to differences in helix *α*1 (Figures 2 and S3). Instead of using its N-terminus for oligomerization, EcPAPSR's homodimeric interface is formed using helices *α*4 and *α*5 (MtbAPSR numbering, Figure 3B). Although *α*4 and *α*5 of MtbAPSR are of similar lengths to those helices in EcPAPSR, the sequence of MtbAPSR is not compatible with the dimer interface formation (Figure 3B). Like EcPAPSR, PaAPSR uses helix *α*5 in oligomerization, but unlike EcPAPSR, PaAPSR is a homotetramer (Figure 3A).

The comparison between PaAPSR and MtbAPSR warrants a more detailed description as PaAPSR has the highest structural similarity to MtbAPSR (*Z*-score = 24.8; rmsd = 2.1 Å for 199 C*α* atoms) and is the only other [4Fe−4S] cluster-containing APSR enzyme with a structure solved. The main structural differences are that MtbAPSR has a longer *α*1 helix and a longer flexible loop (G40 to C59) between *α*2 and *β*1 in comparison with PaAPSR (Figures 4 and S3A). In contrast, PaAPSR has a longer loop between *β*5 and *β*6 than MtbAPSR, and this loop occupies a similar position as the *α*1 extension of MtbAPSR (Figure 4). Additionally, MtbAPSR has a different conformation for *α*5 and a longer *β*3 strand in comparison

https://doi.org/10.1021/acsomega.1c01043
ACS Omega 2021, 6, 13756−13765

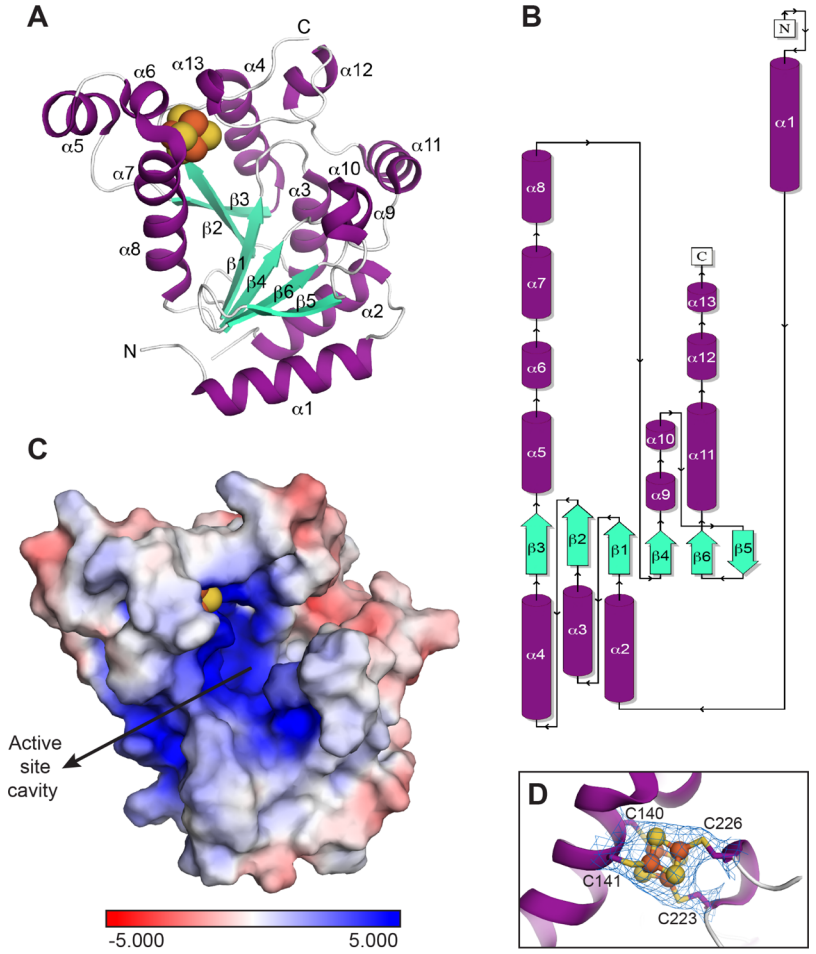

Figure 1. Crystal structure of MtbAPSR. (A) Overall structure of the MtbAPSR functional monomer. The monomer is composed of one domain with a central β-sheet (green) surrounded by α-helices (purple). The [4Fe−4S] cluster is shown in orange (Fe) and yellow (S) spheres. N and C represent the N-terminus and the C-terminus, respectively. The stereoview is shown in Figure S1. (B) Topology diagram of MtbAPSR. The topology was generated using PDBSum[14] and manually edited for consistency with (A). (C) Electrostatic surface potential representation of the MtbAPSR monomer. Positive and negative charges are indicated in blue and red, respectively. (D) The [4Fe−4S] cluster coordinated to four cysteine residues (C140, C141, C223, and C226). The blue mesh represents the $2F_o - F_c$ electron density map contoured at 1.5 σ for the [4Fe−4S] cluster [orange (Fe) and yellow (S) spheres] and four cysteine side chains.

with PaAPSR (Figure 4). Because β3 and α5 of PaAPSR stabilize its tetrameric interface[8] (Figure 3A), the alterations in β3, α5, and α1 of MtbAPSR may explain its inability to tetramerize. Unfortunately, the lack of density following residue 231 of MtbAPSR does not allow us to compare the structural features at the C-termini to that of the PaAPSR enzyme, which is more fully visualized. However, conservation of residues (Figure 4A) suggests that the structures will be similar.

Active Site of MtbAPSR. Soaking crystals of MtbAPSR with substrate APS gives rise to a 3 sigma $F_o - F_c$ difference omit electron density that is consistent with APS being bound to the enzyme in both monomers in the asymmetric unit (Figure 5A,B). The active site of MtbAPSR is located in a positively charged deep cavity in the center of the protein (Figures 1C and 5A), where the substrate sits on the C-terminal end of β1, β2, β4, and α9 and interacts with six residues (A64, S65, L88, G162, D167, and I221) and two water molecules (Figures 5D and S4). The interactions between APS and the enzyme involve the residues' main chain, except for D167. The adenine ring of APS hydrogen bonds to L88 and S65, the ribose ring makes hydrogen bonds with A64 and G162, the phosphate group hydrogen bonds to the D167 side chain and a water molecule, and the sulfate group hydrogen bonds to I221 and a water molecule and is located 8.5 Å away from the [4Fe−4S] cluster (Figure 5D).

The crystal structure of MtbAPSR soaked with product AMP shows a 3 sigma $F_o - F_c$ difference omit electron density for AMP being bound in the active site in both monomers of the asymmetric unit (Figure 5C). It occupies the same binding site as APS (Figure 5A) and interacts with the same residues that are involved in binding APS, except for I221, and a water molecule (Figures 5E and S4).

Structural comparisons between MtbAPSR, PaAPSR, and ScPAPSR active sites show that APS, AMP, and PAP have similar binding modes (Figures 6 and S5). Two structures are available (Table 1) that depict substrate APS binding, MtbAPSR and PaAPSR, and their structural comparison reveals very similar binding interactions (Figure 6A). Notably, all active site residues S65, L88, K145, G162, I221, R237, and R240 are conserved between MtbAPSR and PaAPSR enzymes (Figure 4A). Unfortunately, the disorder in the C-terminus of MtAPSR prevents us from observing the interactions made between the APS sulfate group and R237 and R240 (MtbAPSR

https://doi.org/10.1021/acsomega.1c01043
ACS Omega 2021, 6, 13756−13765

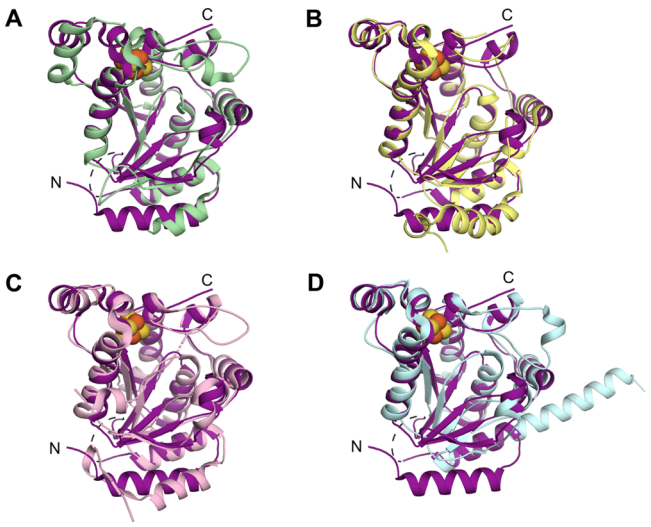

Figure 2. Structural comparisons between MtbAPSR and related structures. (A) Superposition between MtbAPSR (purple) and PaAPSR (green; PDB code 2GOY[8]) monomers. The dashed line is the missing loop between α2 and β1 in MtbAPSR. (B) Superposition between MtbAPSR (purple) and EcPAPSR (yellow; PDB code 2O8V[9]) monomers. (C) Superposition between MtbAPSR (purple) and ScPAPSR (pink; PDB code 2OQ2[10]) monomers. (D) Superposition between MtbAPSR (purple) and PpAPSR-B (light blue; PDB code 4BWV[16]) monomers. N represents the N-terminus, and C represents the C-terminus. The [4Fe−4S] cluster is shown in orange (Fe) and yellow (S) spheres for MtbAPSR and PaAPSR structures. A stereoview version of this figure is available in the Supporting Information (Figure S3).

numbering), which is visualized in the PaAPSR structure (Figure 6A). R237 and R240 are part of a conserved ^{237}R(S/E/A)GR(W/F)^{241} motif (Mtb numbering), and due to this conservation, we believe that contacts with these residues will be made in MtbAPSR when the C-terminal tail is ordered. In the absence of an ordered C-terminal tail and contacts with R237 and R240 to hold the phosphosulfate moiety in a higher position in the active site, the phosphosulfate moiety sinks down to a position where it can interact with the I221 main chain and D167 side chain (Figure 6A). In the newly observed conformation, the sulfate group of APS does not make a hydrogen bond with K145, whereas APS in the PaAPSR structure does (Figure 6A). Importantly, the substitution of K145 to alanine in MtbAPSR results in an enzyme variant that has a lower activity and reduced substrate binding,[12] indicating that K145 plays a role in both APSR enzymes. The "lower" position of phosphosulfate observed in MtbAPSR is only likely to occur when the C-terminal tail is not situated over the active site since the "lower" position is missing all favorable electrostatic interactions for APS and would not be expected to be competitive with the "upper" position that is observed in PaAPSR when the C-terminal tail is available. In the case of product AMP, however, the presumed lower-affinity "lower" active site position would enable product release.

The crystal structure of ScPAPSR provides another view of product binding; in this case, the product is PAP.[10] Importantly, this structure of the five compared here has the most complete view of the C-terminal tail (only the last four residues are disordered). As was observed in the PaAPSR structure, R240 and R237 (Mtb numbering) of the C-terminal tail of ScPAPSR are positioned toward the binding site for the 5′-phosphosulfate moiety (Figure 6B), but since this is a product-bound structure, sulfate is not there. The position of 5′-phosphate of PAP is similar to what we observe for 5′-phosphate of MtbAPSR's product AMP moiety (Figures 6B and S5). Notably, the ScPAPSR structure allows us to visualize another conserved catalytic motif ^{248}E<u>C</u>G(L/I)H^{252} (Mtb numbering; Figure S2). The superposition between MtbAPSR, PaAPSR, and ScPAPSR active sites indicates that conserved catalytic C249 is located close enough to the sulfate group of APS for catalysis when APS is positioned as it is in the PaAPSR

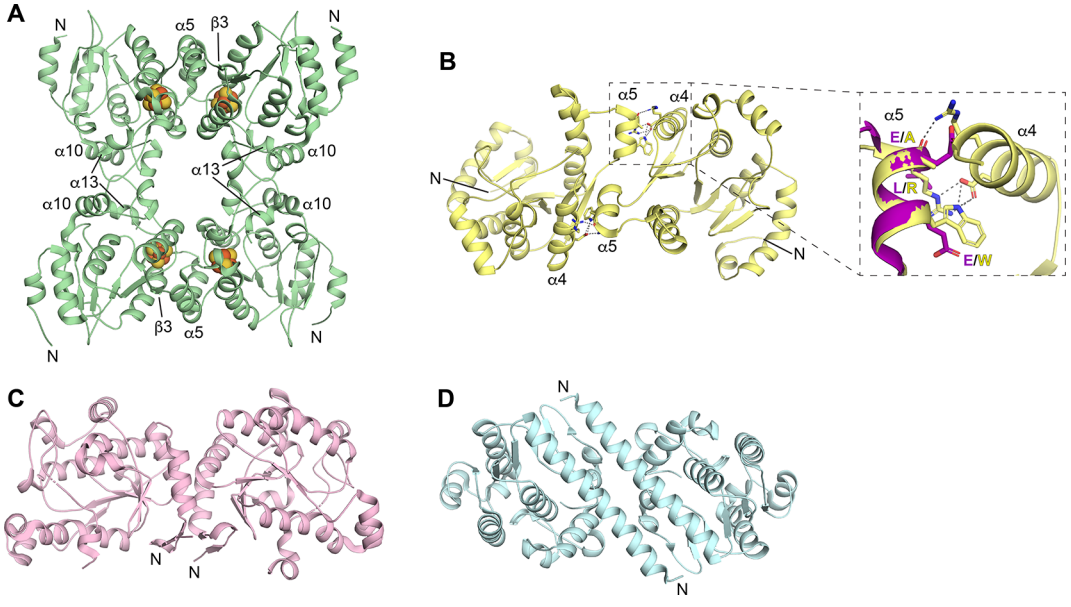

Figure 3. APSR and PAPSR oligomeric states. (A) PaAPSR homotetramer (PDB code 2GOY). The [4Fe−4S] cluster is shown in orange (Fe) and yellow (S) spheres. (B) EcPAPSR homodimer (PDB code 1SUR) with residues that contribute to the dimer interface in EcPAPSR in yellow. The zoomed-in box shows that residues in MtbAPSR (purple) are not compatible with dimer formation. (C) ScPAPSR homodimer (PDB cod 2OQ2). (D) PpAPSR-B homodimer (PDB code 4BWV). N represents the N-terminus.

https://doi.org/10.1021/acsomega.1c01043
ACS Omega 2021, 6, 13756−13765

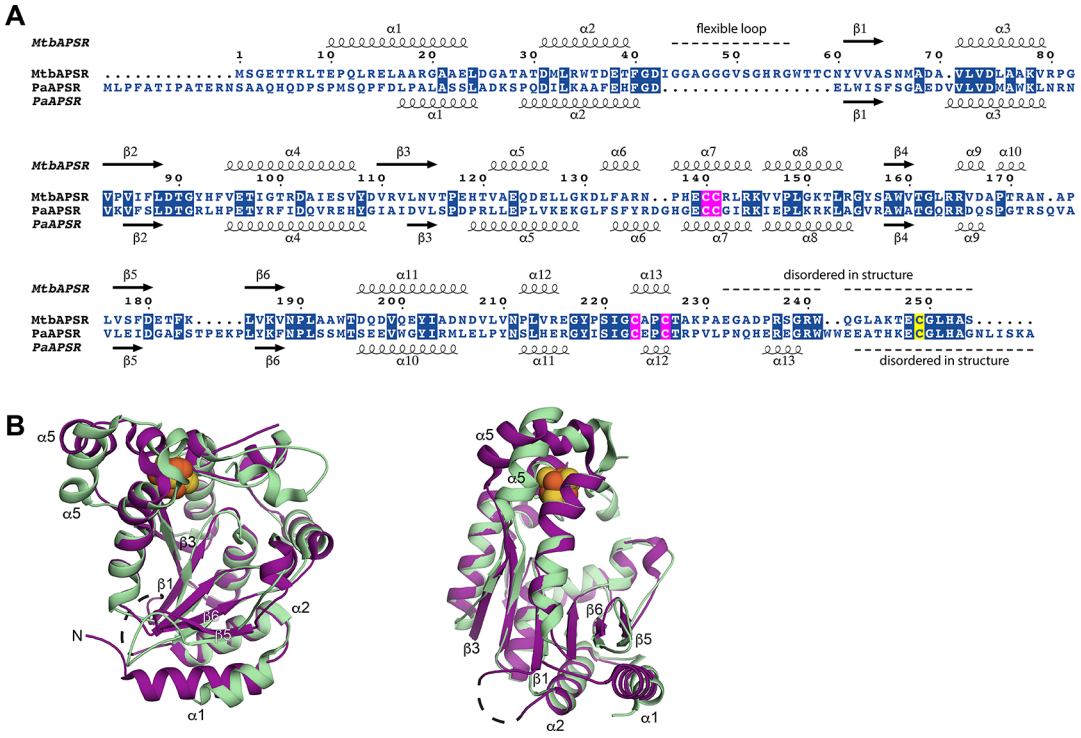

Figure 4. Structural comparisons of MtbAPSR and PaAPSR. (A) Sequence alignment based on the structures of MtbAPSR and PaAPSR. The conserved residues are indicated in the blue boxes. The four conserved cysteine residues, which are shown to bind an [4Fe−4S] cluster, are indicated in magenta boxes. Conserved catalytic cysteine is indicated in the yellow box. Secondary structures of MtbAPSR and PaAPSR are shown on the top and the bottom of the sequence alignment, respectively. The alignment is graphically displayed using ESPript (https://espript.ibcp.fr/ESPript/cgi-bin/ESPript.cgi). (B) Two orthogonal views of the superposition between MtbAPSR (purple) and PaAPSR (green; PDB code 2GOY) monomers. The [4Fe−4S] cluster is shown in orange (Fe) and yellow (S) spheres. N represents the N-terminus. The MtbAPSR flexible loop between α2 and β1 is shown as a dashed black line.

structure, that is, the "upper" position (Figure 6B). C249 is located 3.3 and 5.5 Å away from the sulfur atom of APS in PaAPSR and MtbAPSR, respectively. The ScPAPSR structure also shows how close K145 can get to C249 (Mtb numbering) when the C-terminal tail is fully ordered (Figure 6B). In the ScPAPSR structure, K145 is moved away from C249 toward the position that is occupied by the [4Fe−4S] cluster in the Mtb and PaAPSR structures. It is tempting to propose that, in addition to interacting with the sulfate group of APS/PAPS, K145 could activate C249 for catalysis, consistent with the lower activity reported for the K145A MtbAPSR variant.[12] Additionally, when the C-terminal tail is fully ordered, conserved H252 is in close proximity to endocyclic ribose oxygen and the 5′-phosphate group of APS, AMP, PAP, and PAPS. The substitution of H252 with alanine in MtbAPSR decreases the substrate affinity,[18] indicating that H252 likely adopts the same position in MtbAPSR.

Collectively, the ScPAPSR, PaAPSR, and MtbAPSR structures indicate that the conserved C-terminal motifs ^{237}R(S/E/A)GR(W/F)^{241} and ^{248}ECG(L/I)H^{252} (Figure S2) are required for the proper positioning of substrate APS in the active site for catalysis, although not essential for APS/PAPS and AMP/PAP binding. Together, sequence conservation data and the structural snapshots with various degrees of ordering of the C-terminal tail and different substrates and products bound suggest that the substrate and product binding modes and catalytic mechanisms of APSR and PAPSR are analogous. Thus, despite substrate differences, oligomeric state differences, the presence or absence of a [4Fe−4S] cluster, and the modest sequence conservation, the core structures of the active sites are very similar. In terms of drug design targeting MtbAPSR, therefore, structural data from all of these APSR and PAPSR enzymes should be considered collectively as they inform us about the size, shape, and properties of a small molecule that could anchor the C-terminal tail over the active site cavity and thus seal the active site and inhibit the enzyme.

CONCLUSIONS

In this work, we describe the crystal structure of MtbAPSR, which will facilitate inhibitor design and allow for an inhibitor-based validation of MtbAPSR as a drug target against TB. Our MtbAPSR structures in a complex with APS and AMP show that the substrate and product have similar binding modes to each other and to substrate- and product-bound structures of other APSRs and PAPSRs of known structure. The structural comparisons described here provide a framework for structure-based drug design to combat TB by taking advantage of the first committed step in sulfate assimilation.

MATERIALS AND METHODS

Expression and Purification. The MtbAPSR gene was previously cloned in a pET-24b(+) vector under the control of a T7 promoter.[19] The plasmids pET24b-MtbAPSR and pDB1282-isc-operon, which contains the iscS, iscU, iscA, hscB, hscA, and fdx portions of the isc (iron−sulfur cluster) operon from *Azotobacter vinelandii* under the control of an arabinose promoter (a kind gift from Dr. Dennis Dean, Virginia Tech, Blacksburg, VA), were cotransformed into *E. coli* BL21(DE3). Cells containing both pET24b-MtbAPSR and pDB1282-isc-operon plasmids were isolated from Luria broth

https://doi.org/10.1021/acsomega.1c01043
ACS Omega 2021, 6, 13756−13765

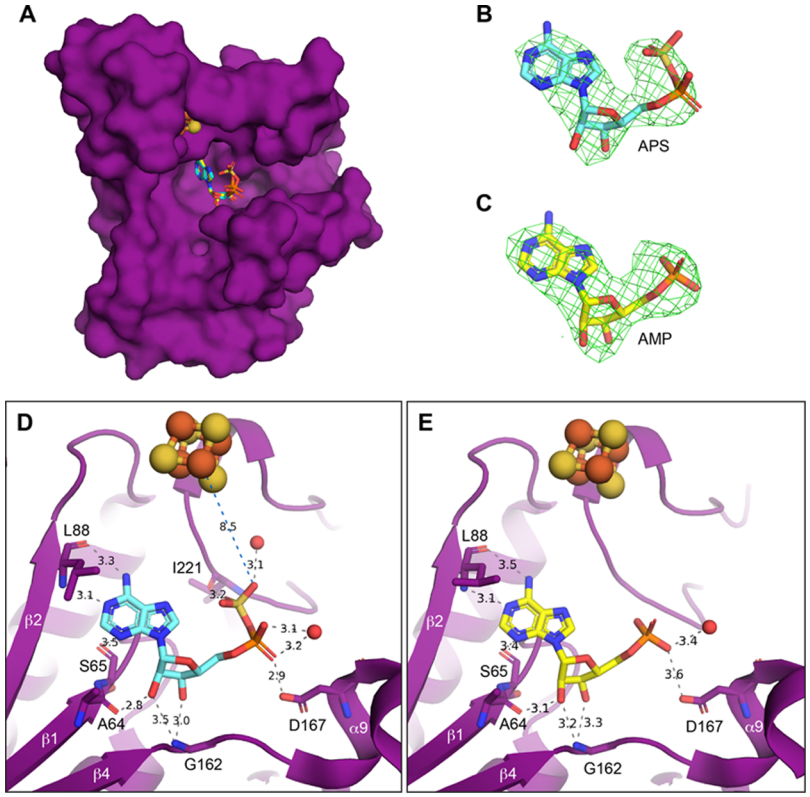

Figure 5. MtbAPSR active site with substrate APS and product AMP bound. (A) Superposition of APS (cyan) and AMP (yellow) in the deep active site cavity of MtbAPSR (purple surface). (B) MtbAPSR in a complex with APS. The $F_o - F_c$ difference omit electron density map contoured at 3.0 rmsd for APS (cyan) is shown as a green mesh. (C) MtbAPSR in a complex with AMP. The $F_o - F_c$ difference omit electron density map contoured at 3.0 σ for AMP (yellow) is shown as a green mesh. (D) Interactions between APS (cyan) and the active site residues in MtbAPSR (purple). The distance (8.5 Å) between sulfate oxygen of APS and the Fe atom of the [4Fe−4S] cluster is shown as a blue dashed line. (E) Interactions between AMP (yellow) and the active site residues in MtbAPSR (purple). The [4Fe−4S] cluster is shown in orange (Fe) and yellow (S) spheres. The water molecules are shown in red spheres.

(LB) agar plates containing 50 μg/mL kanamycin and 100 μg/mL carbenicillin. A single colony was used to inoculate 10 mL of the LB medium supplemented with antibiotics (50 μg/mL kanamycin and 100 μg/mL carbenicillin), and the culture was grown for 16 h at 37 °C and 190 rpm. This culture was 1:100 diluted with LB plus antibiotics and grown at 37 °C and 190 rpm until the absorbance at 600 nm reached 0.5−0.6. At this point, 0.2% (w/v) arabinose, 0.8 mM iron citrate, and 2 mM L-cysteine were added, and the culture was grown for 1 h at 37 °C and 190 rpm. The cells were then induced with 0.3 mM isopropyl β-D-thiogalactopyranoside (IPTG) and grown for 16−18 h at 18 °C and 70 rpm. The cells were harvested by centrifugation (5000×g for 10 min) and the pellets stored at −20 °C.

Recombinant C-terminal His-tagged MtbAPSR was purified by nickel affinity and size exclusion chromatography at 4 °C in an MBraun anerobic glovebox. Briefly, the pellet from 1 L of the culture was resuspended in 40 mL of buffer A [50 mM monosodium phosphate, 300 mM NaCl, pH 8.5, 1 mM dithiothreitol (DTT)] with 1 tablet of the EDTA-free protease inhibitor cocktail (cOmplete; Millipore Sigma) and lysed by sonication for 10 min (amplitude 5, 1 s pulse on and 2 s pulse off; QSonica sonicator). The lysate was centrifuged for 30 min at 14,100×g and loaded into a 5 mL HisTrap HP His tag column (GE Healthcare Life Sciences) previously equilibrated in buffer A. The column was then washed with a step gradient of imidazole from 0 to 50 mM in buffer A. Recombinant MtbAPSR was eluted with buffer A plus 100 mM imidazole, and the purity of the protein was checked by 12% SDS-PAGE (Bio-Rad). Fractions containing MtbAPSR were pooled, concentrated by centrifugation (10 kDA Amicon Ultra; Millipore Sigma), and loaded into a 16/60 Superdex 75 size exclusion column (GE Healthcare Life Sciences) previously equilibrated in buffer B (50 mM HEPES, pH 7.2, 150 mM NaCl, 5 mM DTT). The protein concentration was determined using the extinction coefficient at 280 nm (ε_{280} = 36,815 M^{-1} cm^{-1}), which was determined from amino acid composition (https://web.expasy.org/protparam/).

Crystallization. Initial MtbAPSR crystallization conditions were identified using a Mosquito robot (TTP Labtech) and optimized using a sitting drop vapor diffusion method, both at 20 °C in an MBraun anaerobic glovebox. Drops were prepared by mixing 1 μL of the protein solution (16−30 mg mL^{-1} in 50 mM HEPES, pH 7.2, 150 mM NaCl, 5 mM DTT) and 1 μL of the reservoir solution [0.1 M MES pH 6−6.5, 10−12% (v/v) polyethylene glycol (PEG) 20,000] and equilibrated against 400 μL of the reservoir solution. After 1 day, brownish crystals were obtained. The crystals were transferred to a cryoprotectant solution (25% glycerol, 18% PEG 20,000, 0.1 M MES pH 6−6.5), and flash-cooled in liquid nitrogen in the Coy anaerobic chamber. Crystals of MtbAPSR bound to APS and AMP were obtained by quick-soaking in a cryoprotectant solution with 5 mM APS and 10 mM AMP, respectively, and flash-cooled in liquid nitrogen in the Coy chamber.

Data Collection and Structure Determination. Data collection was performed at the 24-ID-C beamline of the

https://doi.org/10.1021/acsomega.1c01043
ACS Omega 2021, 6, 13756−13765

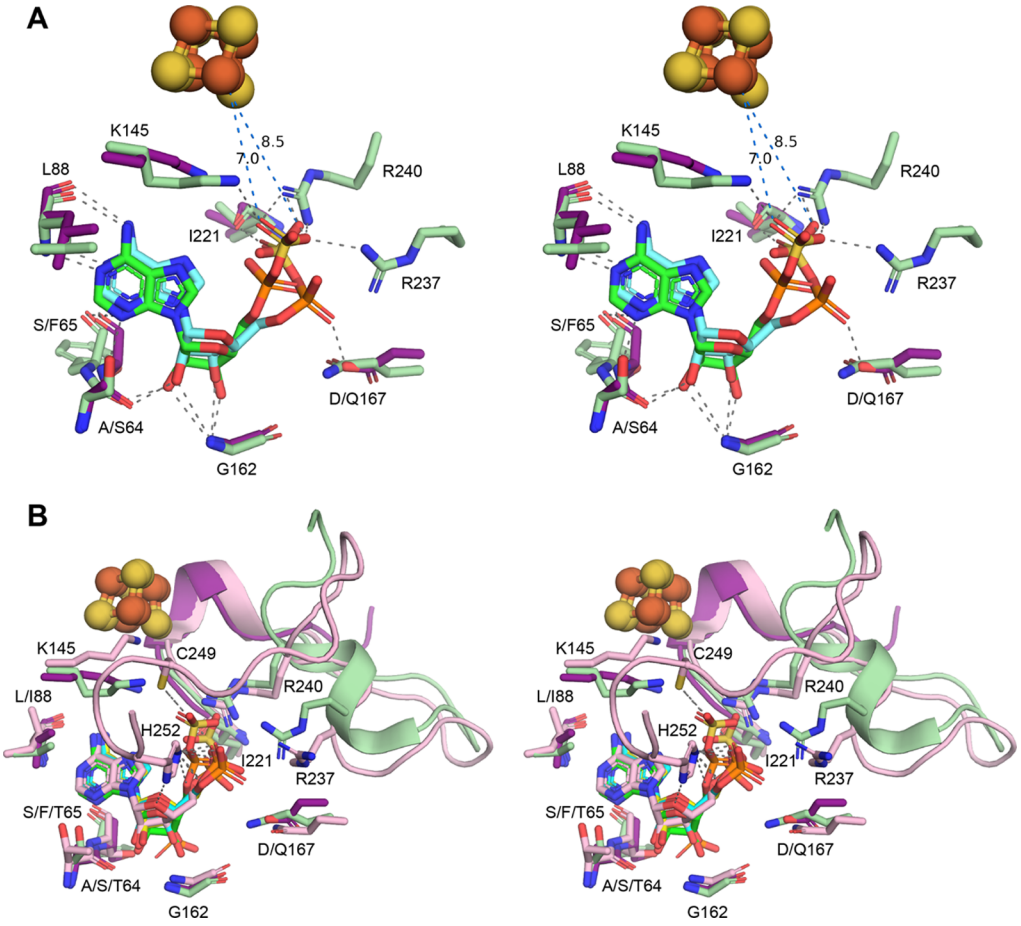

Figure 6. Structural comparisons between MtbAPSR, PaAPSR, and ScPAPSR active sites. (A) Stereoview of the superposition between MtbAPSR (purple) and PaAPSR (light green; PDB code 2GOY[8]) active sites. Substrate APS is shown in cyan and green for MtbAPSR and PaAPSR structures, respectively. The distances (7 and 8.5 Å) between sulfate oxygen of APS and the Fe atom of the [4Fe−4S] cluster are shown as blue dashed lines. (B) Stereoview of the superposition between MtbAPSR (purple), PaAPSR (light green; PDB code 2GOY[8]), and ScPAPSR (pink; PDB code 2OQ2[10]) active sites. Substrate APS is shown in cyan (MtbAPSR) and green (PaAPSR). The products AMP and PAP are shown in yellow (MtbAPSR) and pink (ScPAPSR), respectively. The C-terminal tail is shown as a cartoon representation. The [4Fe−4S] cluster is shown in orange (Fe) and yellow (S) spheres.

Advanced Photon Source. An Fe-SAD dataset was collected using an inverse-beam method with Friedel pairs measured by rotating the crystal 180° every 40 frames with a 0.5° oscillation and an exposure time of 0.5 s. Diffraction data were processed and scaled using HKL2000[20] with the CC1/2 value used to determine the resolution cutoff. The crystal structure of MtbAPSR was solved by Fe-SAD. The positions of seven Fe sites per dimer were determined and refined using phenix.autosol.[21] A partial model was built in Coot[22] using a 4 Å resolution experimental map with a figure of merit of 0.487, followed by model building using phenix.autosol using a 3.45 Å resolution experimental map that had a figure of merit of 0.478. Native data from 50 to 3.1 Å resolution were used for structure refinement and iterative rounds of model building and addition of water molecules in Coot.[22]

The crystal structures of MtbAPSR in a complex with substrate APS and product AMP were solved by molecular replacement techniques implemented in Phaser[23] using coordinates of the MtbAPSR structure determined by Fe-SAD. Following molecular replacement, simulated annealing was performed in phenix.refine[21] to remove the model bias. The models were refined by iterative rounds of model building and addition of water molecules using Coot.[22] Refinement of all three structures in phenix.refine[21] used noncrystallographic symmetry restraints, TLS (translation, libration, and screw), and positional and B-factor refinement, with APS and AMP geometry restraints generated by phenix.elbow.[21] The data collection and refinement statistics are summarized in Table 2. The residues visualized in each structure, of 254 residues, are listed in Table S1. Figures were created with PyMol software.[24] The electrostatic surface potential was calculated using the adaptive Poisson−Boltzmann solver (APBS)[25] plugin implemented in PyMol, using default parameters. Crystallographic software packages were compiled by SBGrid.[26]

■ ASSOCIATED CONTENT

Supporting Information

The Supporting Information is available free of charge at https://pubs.acs.org/doi/10.1021/acsomega.1c01043.

Number of residues visualized in each MtbAPSR structure, stereoview of the MtbAPSR monomer, sequence alignment of APSR and PAPSR enzymes, stereoview version of Figure 2, stereoview of the superposition of substrate APS and product AMP in the active site of MtbAPSR, and stereoview of the

https://doi.org/10.1021/acsomega.1c01043
ACS Omega 2021, 6, 13756−13765

superposition of APS, AMP, and PAP in the active sites of PaAPSR, MtbAPSR, and ScPAPSR (PDF)

Accession Codes

The structures of holo-MtbAPSR, bound to substrate APS and bound to product AMP have been deposited in the Protein Data Bank as entries 7LHR, 7LHS, and 7LHU, respectively.

AUTHOR INFORMATION

Corresponding Author

Catherine L. Drennan − *Howard Hughes Medical Institute, Department of Biology, and Department of Chemistry, Massachusetts Institute of Technology, Cambridge, Massachusetts 02139, United States;* orcid.org/0000-0001-5486-2755; Email: cdrennan@mit.edu

Authors

Patricia R. Feliciano − *Howard Hughes Medical Institute, Department of Biology, and Department of Chemistry, Massachusetts Institute of Technology, Cambridge, Massachusetts 02139, United States;* orcid.org/0000-0003-3853-115X

Kate S. Carroll − *Department of Chemistry, The Scripps Research Institute, Jupiter, Florida 33458, United States;* orcid.org/0000-0002-7624-9617

Complete contact information is available at: https://pubs.acs.org/10.1021/acsomega.1c01043

Funding

This work was supported by the National Institute of General Medical Sciences of the National Institutes of Health grants R35 GM126982 (C.L.D.) and R01 GM087638 (K.S.C.). C.L.D. is a Howard Hughes Medical Institute investigator. This work is based upon research conducted at the Northeastern Collaborative Access Team beamlines, which are funded by the National Institute of General Medical Sciences of the National Institutes of Health (P30 GM124165). This research used resources of the Advanced Photon Source, a U.S. Department of Energy (DOE) Office of Science User Facility operated for the DOE Office of Science by the Argonne National Laboratory under contract no. DE-AC02-06CH11357.

Notes

The authors declare no competing financial interest.

REFERENCES

(1) Pai, M.; Behr, M. A.; Dowdy, D.; Dheda, K.; Divangahi, M.; Boehme, C. C.; Ginsberg, A.; Swaminathan, S.; Spigelman, M.; Getahun, H.; Menzies, D.; Raviglione, M. Tuberculosis. *Nat. Rev. Dis. Prim.* **2016**, *2*, 16076.

(2) Bhave, D. P.; Muse, W. B., 3rd; Carroll, K. S. Drug targets in mycobacterial sulfur metabolism. *Infect. Disord.: Drug Targets* **2007**, *7*, 140−158.

(3) Senaratne, R. H.; De Silva, A. D.; Williams, S. J.; Mougous, J. D.; Reader, J. R., Jr; Zhang, T.; Chan, S.; Sidders, B.; Lee, D. H.; Chan, J.; Bertozzi, C. R.; Riley, L. W. 5′-Adenosinephosphosulphate reductase (CysH) protects *Mycobacterium tuberculosis* against free radicals during chronic infection phase in mice. *Mol. Microbiol.* **2006**, *59*, 1744−1753.

(4) Buchmeier, N. A.; Newton, G. L.; Koledin, T.; Fahey, R. C. Association of mycothiol with protection of *Mycobacterium tuberculosis* from toxic oxidants and antibiotics. *Mol. Microbiol.* **2003**, *47*, 1723−1732.

(5) Schwenn, J. D.; Krone, F. A.; Husmann, K. Yeast PAPS reductase: properties and requirements of the purified enzyme. *Arch. Microbiol.* **1988**, *150*, 313−319.

(6) Berendt, U.; Haverkamp, T.; Prior, A.; Schwenn, J. D. Reaction mechanism of thioredoxin: 3′-phospho-adenylylsulfate reductase investigated by site-directed mutagenesis. *Eur. J. Biochem.* **1995**, *233*, 347−356.

(7) Carroll, K. S.; Gao, H.; Chen, H. Y.; Stout, C. D.; Leary, J. A.; Bertozzi, C. R. A conserved mechanism for sulfonucleotide reduction. *PLoS Biol.* **2005**, *3*, 1418−1435.

(8) Chartron, J.; Carroll, K. S.; Shiau, C.; Gao, H.; Leary, J. A.; Bertozzi, C. R.; Stout, C. D. Substrate recognition, protein dynamics, and iron-sulfur cluster in *Pseudomonas aeruginosa* adenosine 5′-phosphosulfate reductase. *J. Mol. Biol.* **2006**, *364*, 152−169.

(9) Chartron, J.; Shiau, C.; Stout, C. D.; Carroll, K. S. 3′-Phosphoadenosine-5′-phosphosulfate reductase in complex with thioredoxin: a structural snapshot in the catalytic cycle. *Biochemistry* **2007**, *46*, 3942−3951.

(10) Yu, Z.; Lemongello, D.; Segel, I. H.; Fisher, A. J. Crystal structure of *Saccharomyces cerevisiae* 3′-phosphoadenosine-5′-phosphosulfate reductase complexed with adenosine 3′,5′-bisphosphate. *Biochemistry* **2008**, *47*, 12777−12786.

(11) Carroll, K. S.; Gao, H.; Chen, H.; Leary, J. A.; Bertozzi, C. R. Investigation of the iron-sulfur cluster in *Mycobacterium tuberculosis* APS reductase: implications for substrate binding and catalysis. *Biochemistry* **2005**, *44*, 14647−14657.

(12) Bhave, D. P.; Hong, J. A.; Lee, M.; Jiang, W.; Krebs, C.; Carroll, K. S. Spectroscopic studies on the [4Fe-4S] cluster in adenosine 5′-phosphosulfate reductase from *Mycobacterium tuberculosis*. *J. Biol. Chem.* **2011**, *286*, 1216−1226.

(13) Krissinel, E.; Henrick, K. Inference of macromolecular assemblies from crystalline state. *J. Mol. Biol.* **2007**, *372*, 774−797.

(14) Laskowski, R. A.; Jabłońska, J.; Pravda, L.; Vařeková, R. S.; Thornton, J. M. PDBsum: Structural summaries of PDB entries. *Protein Sci.* **2018**, *27*, 129−134.

(15) Holm, L. DALI and the persistence of protein shape. *Protein Sci.* **2020**, *29*, 128−140.

(16) Stevenson, C. E. M.; Hughes, R. K.; McManus, M. T.; Lawson, D. M.; Kopriva, S. The X-ray crystal structure of APR-B, an atypical adenosine 5′-phosphosulfate reductase from *Physcomitrella patens*. *FEBS Lett.* **2013**, *587*, 3626−3632.

(17) Savage, H.; Montoya, G.; Svensson, C.; Schwenn, J. D.; Sinning, I. Crystal structure of phosphoadenylyl sulphate (PAPS) reductase: a new family of adenine nucleotide α hydrolases. *Structure* **1997**, *5*, 895−906.

(18) Hong, J. A.; Carroll, K. S. Deciphering the role of histidine 252 in mycobacterial adenosine 5′-phosphosulfate (APS) reductase catalysis. *J. Biol. Chem.* **2011**, *286*, 28567−28573.

(19) Williams, S. J.; Senaratne, R. H.; Mougous, J. D.; Riley, L. W.; Bertozzi, C. R. 5 ′-adenosinephosphosulfate lies at a metabolic branch point in mycobacteria. *J. Biol. Chem.* **2002**, *277*, 32606−32615.

(20) Otwinowski, Z.; Minor, W. Processing of X-ray diffraction data collected in oscillation mode. *Methods Enzymol.* **1997**, *276*, 307−326.

(21) Adams, P. D.; Afonine, P. V.; Bunkóczi, G.; Chen, V. B.; Davis, I. W.; Echols, N.; Headd, J. J.; Hung, L.-W.; Kapral, G. J.; Grosse-Kunstleve, R. W.; McCoy, A. J.; Moriarty, N. W.; Oeffner, R.; Read, R. J.; Richardson, D. C.; Richardson, J. S.; Terwilliger, T. C.; Zwart, P. H. PHENIX: a comprehensive Python-based system for macromolecular structure solution. *Acta Crystallogr. Sect. D Biol. Crystallogr.* **2010**, *66*, 213−221.

(22) Emsley, P.; Lohkamp, B.; Scott, W. G.; Cowtan, K. Features and development of Coot. *Acta Crystallogr. Sect. D Biol. Crystallogr.* **2010**, *66*, 486−501.

(23) McCoy, A. J.; Grosse-Kunstleve, R. W.; Adams, P. D.; Winn, M. D.; Storoni, L. C.; Read, R. J. Phaser crystallographic software. *J. Appl. Crystallogr.* **2007**, *40*, 658−674.

(24) Delano, W. L. *The PyMOL Molecular Graphics System*; DeLano Scientific LLC: San Carlos, CA, USA, 2002.

(25) Baker, N. A.; Sept, D.; Joseph, S.; Holst, M. J.; McCammon, J. A. Electrostatics of nanosystems: Application to microtubules and the ribosome. *Proc. Natl. Acad. Sci. U.S.A.* **2001**, *98*, 10037−10041.
(26) Morin, A.; Eisenbraun, B.; Key, J.; Sanschagrin, P. C.; Timony, M. A.; Ottaviano, M.; Sliz, P. Collaboration gets the most out of software. *eLife* **2013**, *2*, e01456.
(27) Chen, V. B.; Arendall, W. B., III; Headd, J. J.; Keedy, D. A.; Immormino, R. M.; Kapral, G. J.; Murray, L. W.; Richardson, J. S.; Richardson, D. C. MolProbity: all-atom structure validation for macromolecular crystallography. *Acta Crystallogr. Sect. D Biol. Crystallogr.* **2010**, *66*, 12−21.

https://doi.org/10.1021/acsomega.1c01043
ACS Omega 2021, 6, 13756−13765